Proceedings of the 9th World Congress on Momentum, Heat and Mass Transfer (MHMT'23)
London, United Kingdom – April, 2024
Paper No. ENFHT 153
DOI: 10.11159/enfht24.153

Data Analysis of Effective Thermal Conductivity Measurements of Sintered Copper Powder of Various Pore and Particle Sizes

Osama M. Ibrahim*[1], Abdullah Almutairi[1], Ahmed H. Al-Saiafi[2]
[1]Department of Mechanical Engineering, College of Engineering and Petroleum, Kuwait University, Kuwait
[2]Kuwait Oil Company (KOC), Ahmadi, Kuwait
osama.ibrahim@ku.edu.kw, abdullah.almutairi1@ku.edu.kw, Asaiafi@kockw.com

Abstract **–** A new semi-empirical correlation for the effective thermal conductivity of porous sintered metal powder was developed based on the parallel, series, and combination of parallel and series heat flow configurations. The Langmuir shape factor concept is introduced to gain insight into the microstructure complexity of porous media. The new correlation reveals the average heat flow areas as potential targets for curve-fitting equations with fitting parameters. The main objective of this study is to use the new correlation to analyze experimental data of effective thermal conductivity measurements of sintered copper powder of various pores and particle sizes. The analysis's findings include relationships for the effective thermal conductivity, Langmuir shape factors, heat transfer areas, and length of heat transfer pathways as functions of porosity. The results of various pore and particle sizes are then presented and compared to quantify the differences in the microstructure features and their impacts on thermal conductivity.

Keywords**:** Porous media, Effective thermal conductivity, Langmuir shape factor, Semi-empirical correlation, Sintered copper powder

1. Introduction

Developing a general formula that reliably predicts the effective thermal conductivity of two-phase porous media is challenging due to the randomness of the solid phase's microstructure and the complexity of assessing the thermal resistance between sintered particles. Therefore, it is common practice to consider both parallel and series heat flow to build models that estimate the effective thermal conductivity of porous media, where porosity is the adjustment factor between the solid and fluid phase thermal conductivities. The equations provided by these models can be used to predict effective thermal conductivity as a function of porosity. In addition, extra fitting factors may occasionally be used to match experimental data and increase accuracy. These models are described in [1-5]. Furthermore, models with various geometrical shapes of porous media have been investigated to demonstrate the importance of the microstructure and interfacial thermal resistance in accurately predicting the porous-media thermal conductivity [6-12]. These models provide equations to estimate the effective thermal conductivity, but they provide little or no insight into the microstructure of the porous media.

This paper uses a new correlation to analyze effective thermal conductivity experimental data of Sintered Copper Powder (SCP) published by Lu et al. [13]. The new correlation, derived by the super-positioning of re-examined parallel and series heat transfer models [14], provides insights into the microstructure characteristics of SCP. First, semi-empirical correlations were developed to predict the effective thermal conductivity of SCP of different pores and particle sizes. Second, the correlations were used to quantify the Langmuir shape factors, average cross-sectional heat transfer areas of each phase, contact area between the two phases, and length of heat transfer pathways as functions of porosity. Finally, the changes in the microstructure features of different pores and particle sizes and their effects on heat conductivity are then quantified and compared.

2. Experimental Data

2.1 Experimental setup

The experimental setup used by Lu et al. [13] was based on Corsan's method [17], developed for measuring thermal conductivity from 10 to 380 W/m-K and a temperature range of 50 to 500°C. A simplified setup diagram is shown in Fig. 1.

On one side of the setup is an electric heater embedded in a copper bar as a heat source; on the other is a continuous coolant flow used as a heat sink. The specimen of interest is the porous copper sample, while the thermal conductivity of the copper reference specimen is 391 W/m-K. The setup is clamped with a compression force and rapped with thermal insulation to minimize the contact thermal resistance and heat loss. Three temperature measurements were recorded, with prespecified spacing, for the test and reference specimen. The intent is to calculate both specimens' temperature gradients (dT/dx) at a steady state. The normalized effective thermal conductivity $\bar{k}_e$ of the porous copper was then calculated using the following equation,

$$\bar{k}_e = \frac{k_e}{k_s} = \frac{(dT/dx)_s}{(dT/dx)_p} \tag{1}$$

where k_s is the thermal conductivity of the copper reference specimen, while $(dT/dx)_s$ and $(dT/dx)_p$ are the temperature gradients in the reference and test specimens, respectively.

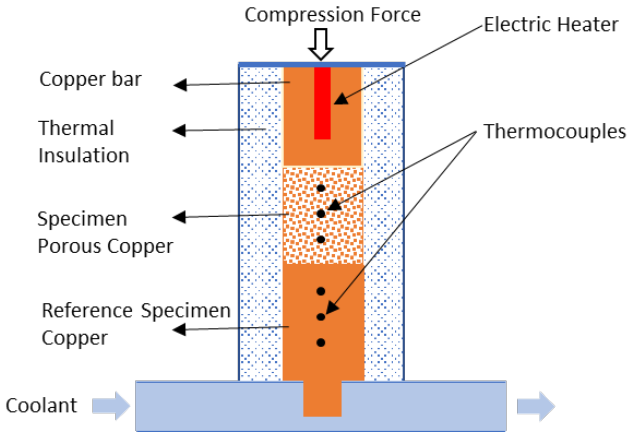

Fig. 1. Simplified diagram of Lu et al. [13] experimental setup.

2.2 Thermal conductivity measurements in vacuum, air, and water vs. pore size

Lu et al. [13] studied the effects of the pore size on the thermal conductivity of SCP in vacuum, air, and water. All SCP samples, in this case, were made of copper powder particle size of 45-47 µm using the "Lost Carbonate Sintering (LCS)" process [15, 16]. As a pore agent, potassium carbonate (K_2CO_3) powder with different size ranges was used to prepare SCP samples of four pore size ranges. The objective was to investigate the impact of the pore size on the effective thermal conductivity.

The effective thermal conductivity measurements in Table 1 are for pore sizes of 250-425 µm and 1000-1500 µm. The effective thermal conductivity values of the SCP with air, water, and vacuum were measured to determine the fluid's contribution. This study evaluated the normalized effective thermal conductivity, assuming pure copper thermal conductivity k_s=391 W/m-K.

Table 1.
For two pore size ranges, effective thermal conductivity measurements of SCP in vacuum, air, and water [13].

250-425 µm						1000-1500 µm					
Vacuum		Air		Water		Vacuum		Air		Water	
P		P		P		P		P		P	
0.619	0.113	0.619	0.116	0.619	0.117	0.595	0.135	0.594	0.139	0.595	0.142
0.633	0.091	0.633	0.094	0.633	0.095	0.632	0.105	0.632	0.112	0.632	0.114
0.69	0.066	0.69	0.07	0.69	0.072	0.702	0.059	0.702	0.069	0.702	0.072

0.726	0.05	0.726	0.055	0.727	0.057	0.747	0.044	0.747	0.054	0.747	0.059
0.764	0.033	0.764	0.038	0.764	0.041	0.778	0.034	0.778	0.045	0.778	0.049

2.3 Thermal conductivity measurements in vacuum vs. copper particle size

Furthermore, Lu et al. [13] examine the impact of copper powder particle size on the effective thermal conductivity of six samples of SCP. The six samples of different particle size ranges were sintered without a pore agent. Particle size range, porosity, and equivalent measurement of the effective thermal conductivity are listed in Table 2. The results show that the particle size affects SCP's ability to transport heat, with particle sizes of 45–70 μm resulting in the maximum effective thermal conductivity.

Table 2.

Measurements of the effective thermal conductivity of SCP for six particle size ranges in vacuum [13].

Particle size range (μm)	10-20	20-45	45-70	75-90	90-150	710-1000
P	0.130	0.140	0.150	0.120	0.120	0.120
$\bar{k}_e$	0.650	0.675	0.716	0.647	0.583	0.532
Uncertainty (%)	+5.6	+13.2	+15.1	+10.1	+7.9	+9.9
	-11.8	-12.2	-14.7	-8.7	-5.0	-7.8

3. Analysis

A new semi-empirical correlation of the effective thermal conductivity that provides more insight into conduction heat transfer in porous media has recently been developed [14]. The new correlation combines re-examined parallel and series heat transfer models. The correlation is presented in terms of four normalized Langmuir shape factors, expressed as,

$$\bar{k}_e = \bar{S}_s^p + \bar{k}_f \bar{S}_f^p + \frac{\bar{k}_f \bar{S}_s^s \bar{S}_f^s}{(\bar{S}_s^s + \bar{k}_f \bar{S}_f^s)} \tag{2}$$

where $\bar{k}$ is the normalized thermal conductivity, $\bar{S}$ is the normalized Langmuir shape factor, superscripts *p* and *s* are referred to as the parallel and series heat transfer models, subscript *e* is referred to the effective thermal conductivity, and subscripts *s* and *f* are referred to the solid and fluid phases.

In Equation 2, the first and second terms stand for heat transfer that occurs in parallel through the solid and fluid phases, whereas the third term denotes heat transfer in series through both phases. Furthermore, Equation 2 reveals four shape factors: two shape factors for parallel heat transfer through the solid and fluid phases and the other two for series heat transfer through the two phases.

The normalized Langmuir shape factors are derived in terms of porosity, the cross-sectional areas of each phase, and the contact area between two phases, as follows,

Parallel heat transfer:

Solid-phase Langmuir shape factor

$$\bar{S}_s^p = \frac{S_s^p}{S} = \frac{(\bar{A}_s^{p\,2})}{(1-P)} \tag{3}$$

Solid-phase Langmuir shape factor

$$\bar{S}_s^p = \frac{S_s^p}{S} = \frac{(\bar{A}_s^{p\,2})}{(1-P)} \tag{4}$$

Series heat transfer:

Solid-phase Langmuir shape factor

$$\bar{S}_s^s = \frac{S_s^s}{S} = \frac{\bar{A}^{s\,2}}{(1-P)} \tag{5}$$

Fluid-phase Langmuir shape factor

$$\bar{S}_f^s = \frac{S_f^s}{S} = \frac{\bar{A}^{s\,2}}{P} \tag{6}$$

where $\bar{A}_s^p$ and $\bar{A}_f^p$ are the average cross-sectional areas of the solid and the fluid phase, while $\bar{A}^s$ is the contact area between the two phases.

The following equations express the best-fit models for the heat transfer areas:

$$\bar{A}_s^p = (1-P)^n \tag{7}$$

$$\bar{A}_f^p = 1 - \bar{A}_s^p = 1 - (1-P)^n \tag{8}$$

$$\bar{A}^s = aP^m(1-P) \tag{9}$$

The cross-sectional areas of Equations 7 and 8 satisfy the porosity limits for pure solid at $P = 0$ and pure fluid at $P = 1$ for all values of $n \geq 1$; i.e., $\bar{A}_s^p = 1$ and $\bar{A}_f^p = 0$ at $P = 0$, and $\bar{A}_s^p = 0\ and\ \bar{A}_f^p = 1\ at\ P = 1$. Similarly, Equation 9 satisfies the contact area porosity limits for all values of a and m, where $\bar{A}^s = 0$ at $P = 0$ and $P = 1$, indicating no series heat transfer for pure solid and fluid phases. Equation 9 is a symmetrical function when $m = 1$, and unsymmetrical for values of $m \neq 1$ with a maximum contact area between $P = 0$ and 1,

Substituting Equations 7 and 8 in Equations 3 and 4, the two normalized Langmuir shape factors for parallel heat transfer are then expressed in terms of porosity as follows:

$$\bar{S}_s^p = (1-P)^{2n-1} \tag{10}$$

$$\bar{S}_f^p = \frac{(1-(1-P)^n)^2}{P} \tag{11}$$

Furthermore, substituting Equation 8 in Equations 4 and 5, the two normalized Langmuir shapes factors for series heat transfer are expressed in terms of porosity as follows:

$$\bar{S}_s^s = \frac{\left(aP^m(1-P)\right)^2}{1-P} \tag{12}$$

$$\bar{S}_f^s = \frac{\left(aP^m(1-P)\right)^2}{P} \tag{13}$$

where *a*, *m*, and *n* are the fitting parameters.

The lengths of the parallel heat transfer pathways of the solid phase ($\bar{L}_s^p$) and fluid phase ($\bar{L}_f^p$) are then determined by the following equations,

$$\bar{L}_s^p = (1-P)^{1-n} \tag{14}$$

$$\bar{L}_f^p = \frac{P}{1-(1-P)^n} \tag{15}$$

While the lengths of the heat transfer pathways in series of the solid phase ($\bar{L}_s^s$) and fluid phase ($\bar{L}_f^s$) are determined by the following equations,

$$\bar{L}_s^s = \frac{1-P}{1+aP^m(1-P)} \tag{16}$$

$$\bar{L}_f^s = \frac{P}{1+aP^m(1-P)} \tag{17}$$

Equations 14-17 are derived using geometrical relationships between the volume and the heat transfer areas. Details and justification of deriving Equations 2-17 are summarized in Ibrahim et al. [14].

4. Results and Discussion

4.1 Effects of pore size on thermal conductivity

The new correlation was used to analyze the experimental measurements in Table 1 to study the effects of the pore size on the effective thermal conductivity. Specifically, Equations 2-6 were used to obtain the best possible values for the fitting parameters n, a, and m for two ranges of pore sizes. It is relevant to note that the fitting parameters are functions of the microstructure of the porous medium and not the physical properties of the solid and fluid phases. Therefore, the data for vacuum, air, and water were combined for the same pore size range to obtain the corresponding fitting parameters. The best-fitting parameters for the small and large pore size ranges are listed in Table 3. The smaller pore size data result in a slightly more accurate correlation with R2=0.98 and $RMSE = 0.055$, compared to the large pore size data with R^2=0.97 and RMSE=0.079.

Table 3.
Fitting parameters for two pore size ranges

Pore Size Range	n	a	m	R^2	RMSE
250-425 (µm)	1.6557	23.56	4.857	0.98	0.055
1000-1500 (µm)	1.6092	86.57	8.021	0.97	0.079

The normalized effective thermal conductivity for SCP vs. porosity is shown in Fig. 2 for small and large pore size ranges in vacuum, air, and water. The solid lines are for the predicted results by Equation 1, and the data points are the experimental results from Table 1. The effective thermal conductivity decreases with increasing porosity, and the model reasonably fits the experimental data. However, for the large pore size range and porosity greater than 0.75, Equation 1 predicts a notably high effective thermal conductivity for the SCP-water system. As expected, the SCP effective thermal conductivity with water is higher than with air and vacuum.

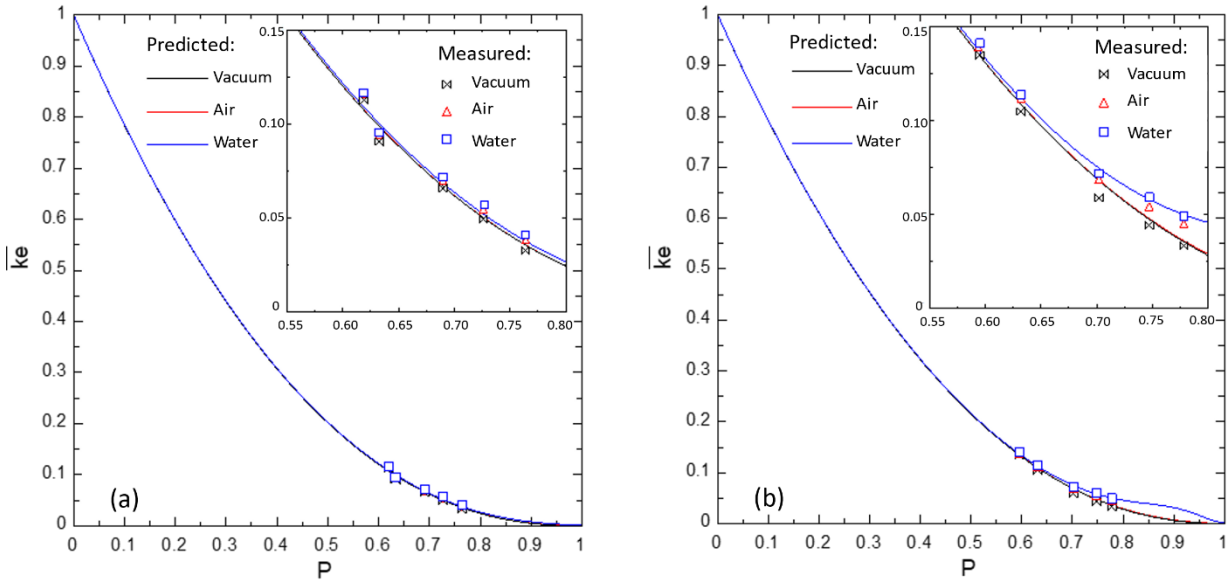

Fig. 2. Effective thermal conductivity measurements and predictions of Equation 1 for two different pore size ranges: (a) 250-425 µm; (b) 1000-1500 µm.

The same data of Fig. 2 is replotted in Fig. 3 to compare the SCP effective thermal conductivity of the two ranges of pore sizes side-by-side in Figs. 3a, 3b, and 3c in vacuum, air, and water, respectively. The results show that the large pore size range has higher effective thermal conductivity for all three cases. The difference between the SCP effective thermal conductivity is higher in the case of water compared to air and vacuum.

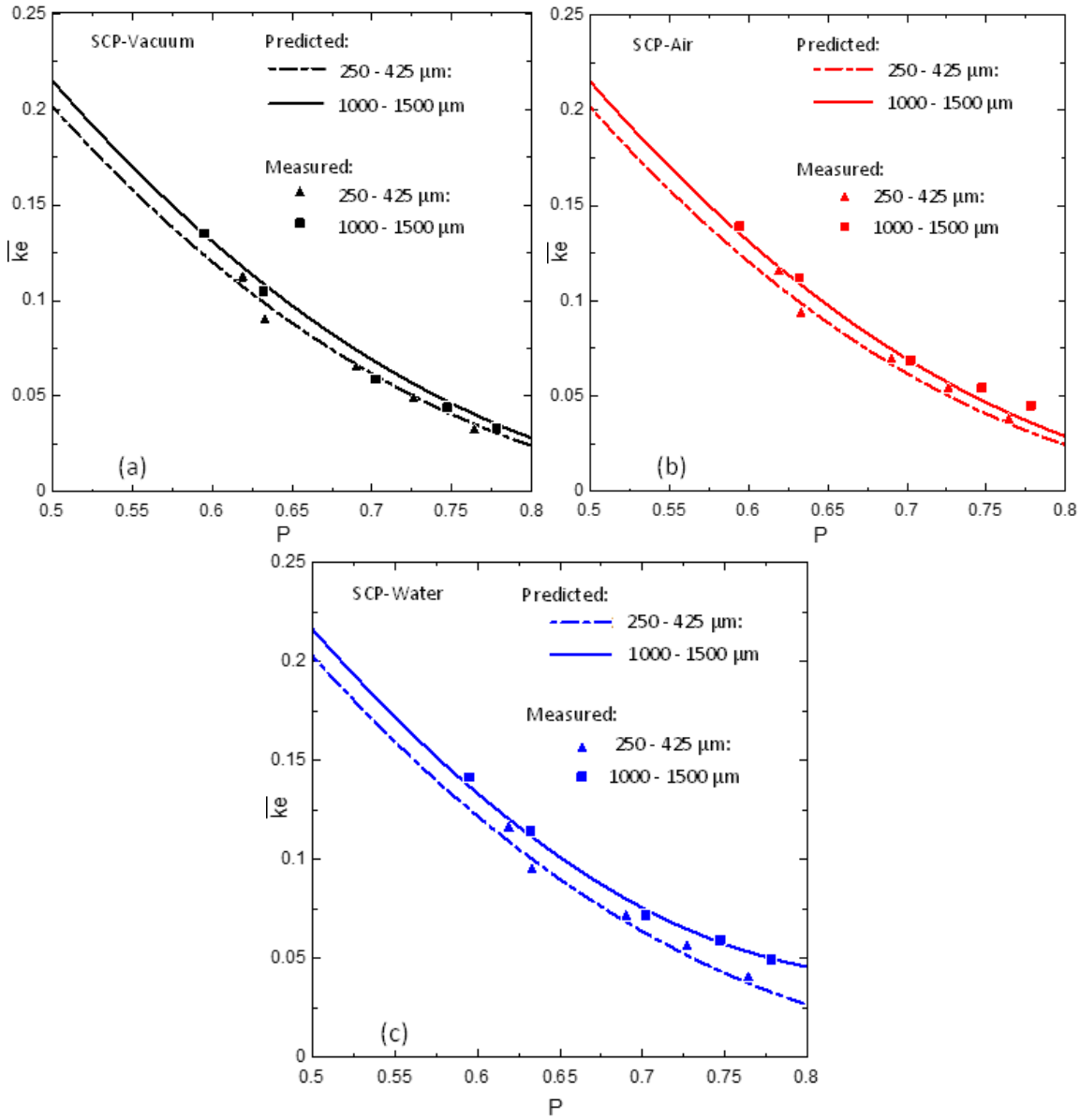

Fig. 3. Comparisons of the SCP effective thermal conductivity of two ranges of pore sizes in (a) vacuum; (b) air; and (c) water.

The normalized cross-sectional and contact areas for the two ranges of pore sizes are shown in Fig. 4. The areas were calculated using Equations 6-8 and the fitting parameters from Table 3 for each size range. The broken lines are for the 250-425 µm pore size range, and the solid lines are for the 1000-1500 µm pore size range. The blue line is for the fluid phase, and the red line is for the solid phase; this plot format was standardized for Figs. 4 - 6.

The average cross-sectional areas, where the parallel heat transfers through the solid and fluid phases, are shown in Fig. 4a. The results show that the large pore size range has a slightly more solid-phase cross-sectional area than the small pore

size range. Since the solid phase, copper, in this case, has much higher thermal conductivity than the fluid phase, any increase in the solid-phase cross-sectional area increases the heat transfer rate and, consequently, higher effective thermal conductivity, as confirmed by Fig. 3.

The normalized contact area, shown in Fig. 4b, is proportional to the heat transferred in series across the system. At $P = 0$ and $P = 1$, the contact area equals zero, affirming no series heat transfer through the pure solid and fluid phases. The contact area for porosity less than 0.35 is small for both pore size ranges. However, the large pore size range has a significantly larger contact area than the small pore size range when the porosity exceeds 0.35, with a maximum value of 3.75 compared to 0.8 at approximately the same porosity of 0.9. Increasing the pore size increases the heat transfer in series through the SCP, especially for high porosity values. This would explain the increase in the effective thermal conductivity of the SCP water system for higher porosities, as shown in Fig. 2b, caused by the higher thermal conductivity of water and the increased contact area, represented by the contribution of the third term of Equation 2.

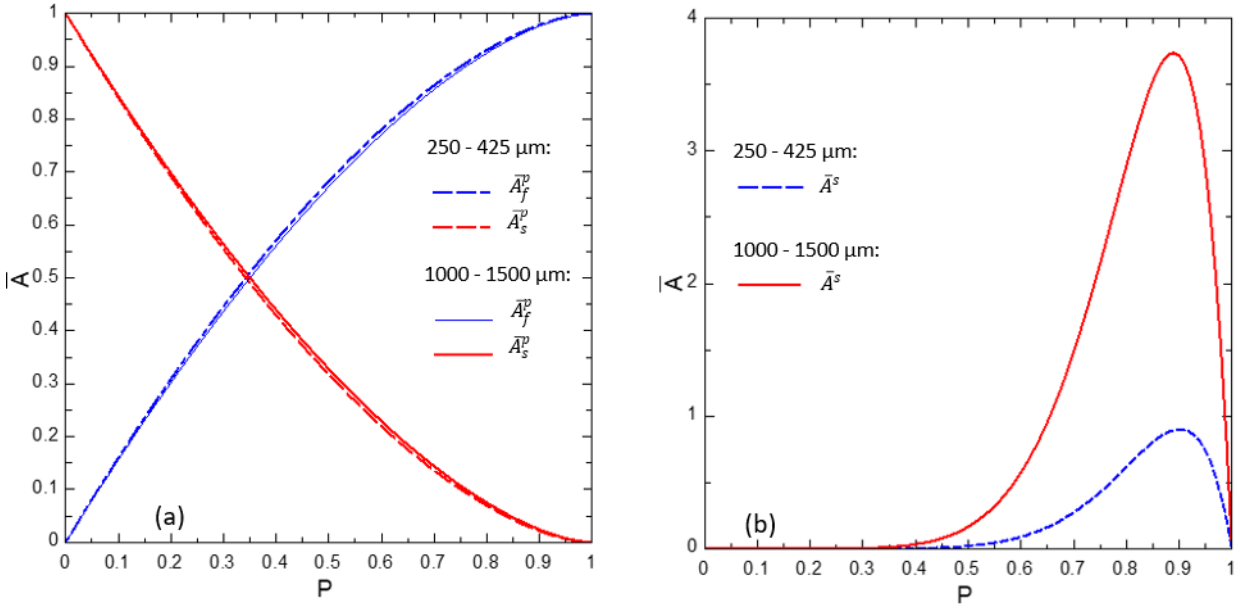

Fig. 4. Heat transfer areas, comparisons between two ranges of pore sizes: (a) Average cross-sectional area of the solid and fluid phases for parallel heat transfer; (b) Contact area between the two phases for series heat transfer.

Figure 5 shows the normalized lengths of the heat transfer pathway in parallel and series of the solid and fluid phases. From Fig. 5a, it can be noticed that heat transferred in parallel takes a longer path in the solid phase than in the fluid phase as the porosity increases. On the other hand, Fig. 5b shows a different pattern where the heat transferred in series in the solid phase takes a longer path up to $P = 0.5$; then, the heat travels longer in the fluid phase. Furthermore, the normalized length of heat transferred in the series of the fluid phase, shown in Fig. 5b, has a drop at $P = 0.9$, and a local minimum, which relates to the maximum contact areas shown in Fig. 3b, i.e., the heat transfer pathways decrease as the contact area increases.

Figure 6 compares the solid-phase and fluid-phase Langmuir shape factors for the two ranges of pore sizes. The parallel models' shape factors, shown in Fig. 6a, follow a similar trend as the cross-sectional areas, while the series model's shape factor, shown in Fig. 6b, follows a similar trend as the contact area. However, there is a slight shift in porosity at the maximum points between the solid and fluid phases.

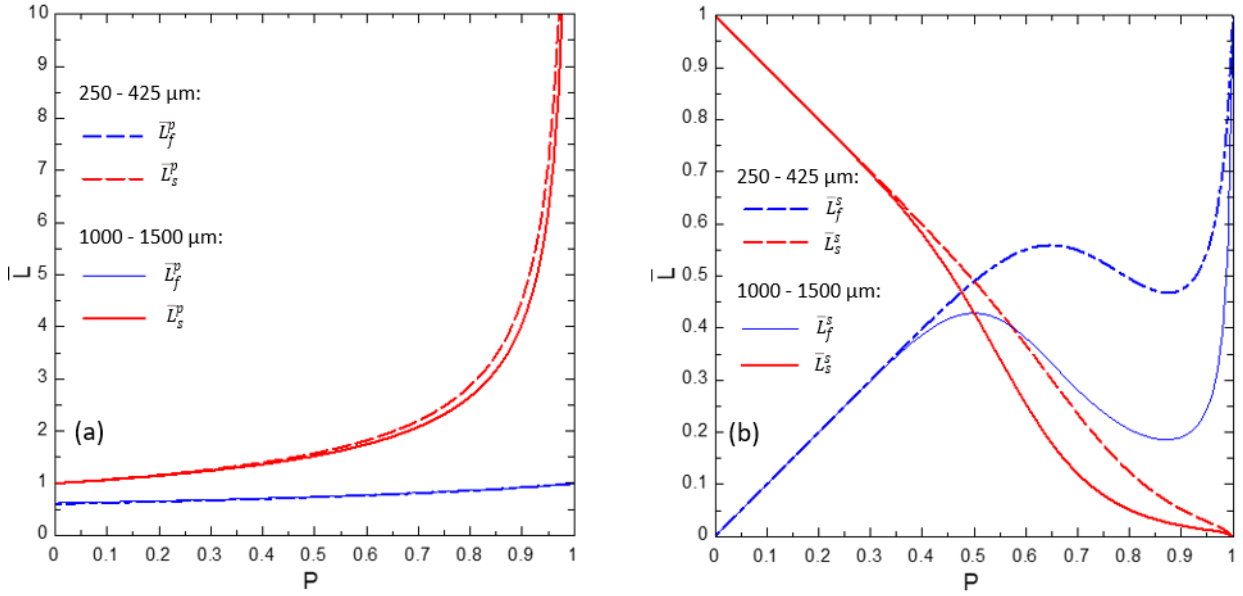

Fig. 5. Heat transfer pathways, comparisons between two ranges of pore sizes: (a) Lengths of heat transfer pathway for parallel heat transfer; (b) Lengths of heat transfer pathways for series heat transfer.

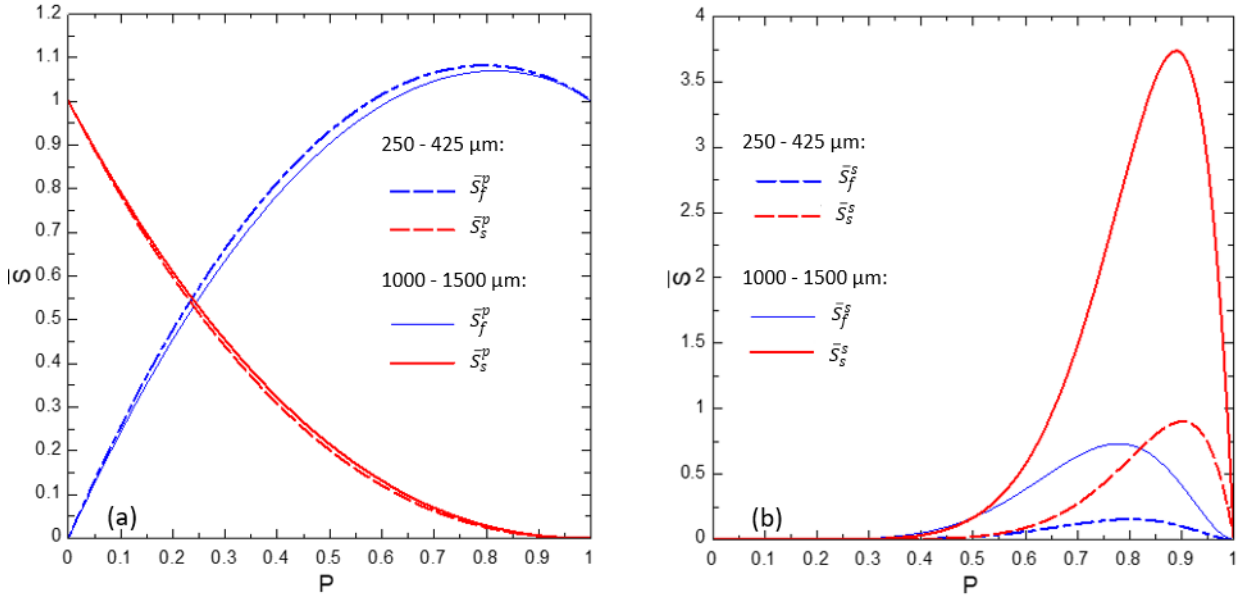

Fig. 6. Langmuir shape factors, comparisons between two ranges of pore sizes: (a) Langmuir shape factors for parallel heat transfer; (b) Langmuir shape factors for series heat transfer.

4.2 Effects of copper powder particle size on thermal conductivity

Further investigation was done by Lu et al. [13] to study the impact of the microstructure due to using different copper particle sizes on thermal conductivity. The normalized effective thermal conductivity measurements for six particle size ranges are listed in Table 2. Since the data are for SCP in vacuum, Equation 2 is simplified to the first term only,

$$\bar{k}_e = \bar{S}_s^p = (1-P)^{2n-1} \quad (19)$$

where n is the only fitting parameter evaluated using the data in Table 2. The solution includes one equation, Equation 19, and one unknown, the fitting parameter n. The results are listed in Table 4 below.

Table 4.
Fitting parameter, n, for each particle size range

Particle size range (μm)	10-20	20-45	45-70	75-90	90-150	710-1000
n	2.1125	1.861	1.582	2.272	2.679	3.0381

Since the experiment was conducted in vacuum, only the average cross-sectional area and the length of the parallel heat transfer pathway for the solid phase were evaluated using Equations 7 and 19 and the fitting parameter n in Table 4. The green columns in Fig. 8 represent the effective thermal conductivity and the solid phase's Langmuir shape factor in parallel heat transfer. The corresponding Langmuir shape factor was not labeled separately in this figure because it equals the normalized effective thermal conductivity for SCP, i.e., $\bar{k}_e = \bar{S}_s^p$.

As mentioned earlier, also shown in Fig. 7, the 45-75 μm particle size range has the maximum thermal conductivity, corresponding to the largest cross-sectional area and the shortest heat transfer pathway in the solid phase. This maximum effective thermal conductivity is a function of the particle size range and other factors, such as the particle size distribution, particle shape, and sintering parameters, which were not discussed in Lu et al.'s paper [13].

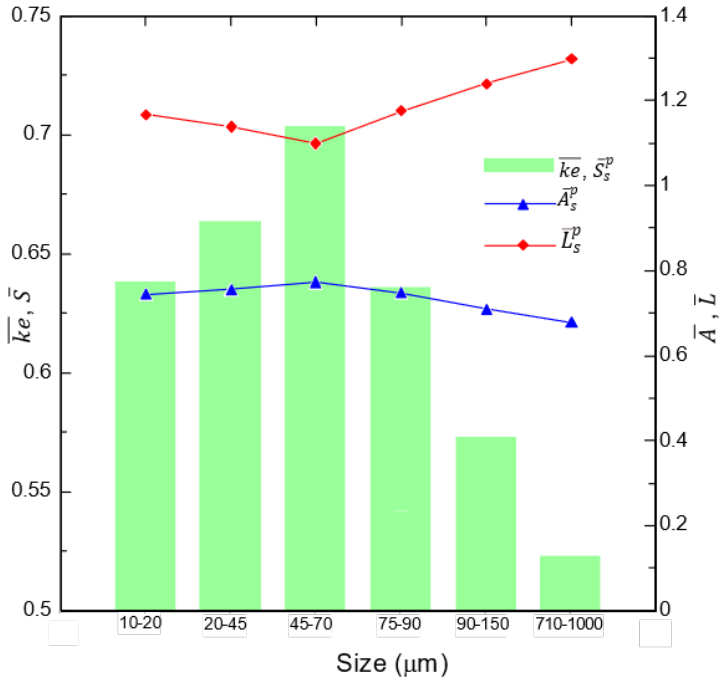

Fig. 7. Normalized effective thermal conductivity ($\bar{k}_e$) in vacuum and the corresponding solid-phase Langmuir shape factor ($\bar{S}_s^p$), average cross-sectional area ($\bar{A}_s^p$), and heat transfer pathway ($\bar{L}_s^p$) vs. particle size.

4.3 Accuracy of the correlation

To estimate the new correlation's accuracy, the deviations from the experimental data were evaluated and plotted in Fig. 8 for the small and large pore size ranges. The data points are for SCP in vacuum, air, and water. Moreover, the deviations of the power model for SCP in vacuum by Lu et al. (2020) were also plotted in Fig. 8. The power model for the normalized effective thermal conductivity is expressed as,

$$\bar{k}_e = \frac{280}{391}(1-P)^{\alpha} \tag{18}$$

where α is the fitting parameter evaluated by Lu et al. [13] for the small and large pore size ranges as $\alpha = 2.02$ for 250-425 μm and $\alpha = 1.939$ for 1000-1500 μm.

The percent deviation of the predicted values of Equation 1 from the experimental measurements is shown in Fig. 8a for the pore size range (250-425 μm) and in Fig. 7b for the large pore size range (1000-1500 μm). The small pore size range predictions are within ±10% compared to ±15% for the large pore size range, excluding one outlier thermal conductivity measurement in air at high porosity. On the other hand, the results from the power law of Equation 18 show relative deviations within the experimental uncertainty reported in Table 2. Equation 18 fits the data reasonably well for the SCP-vacuum case only. It also satisfies the boundary condition at P=1, where $\bar{k}_e = 0$, but it does not meet the boundary condition at $P = 0$, where it yields a value of $\bar{k}_e < 1$. In addition, it does not have terms for the fluid thermal conductivity in parallel or series heat transfer.

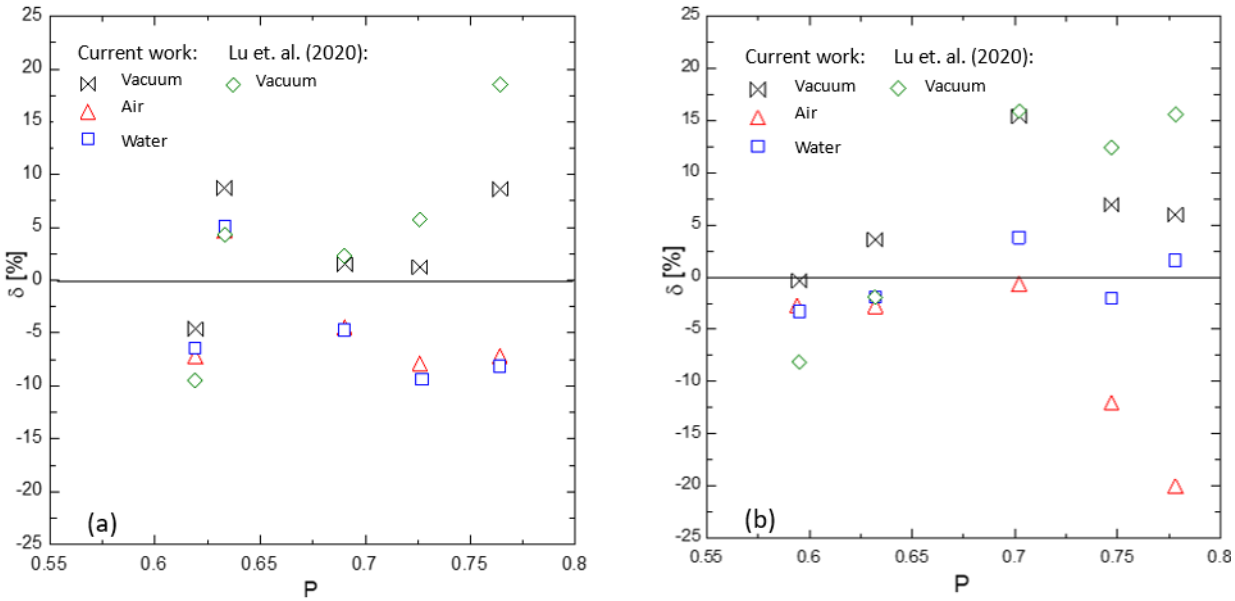

Fig. 8. Percent deviation (δ) of the predicted effective thermal conductivity from the experimental data for two ranges of pore sizes: (a) 250-425 μm; (b) 1000-1500 μm.

5. Concluding Remarks

- Effective thermal conductivity measurements of SCP of the same particle size range and two distinct pore size ranges were analyzed using a novel correlation based on the Langmuir shape factor. The new correlation fitting parameters are functions of the microstructure of porous media and not the physical properties of the solid or fluid phases. Therefore, the effective thermal conductivity measurements in vacuum, air, and water for the same pore size range are pooled to find the best-fitting parameters.
- The analysis results of effective thermal conductivity measurements of samples made of two different pore size ranges show slightly higher solid cross-section areas of the solid phase and considerably higher contact areas between the solid and fluid phases for the larger size range (1000-1500 μm) compared to the small pore size range (250-425 μm)--consequently shorter heat transfer pathways for parallel and series heat transfer, resulting in higher effective thermal conductivity.
- The new correlation was also used to study the impact of copper particle size on the effective thermal conductivity in vacuum for several samples of SCP made of different copper particle size ranges. The analysis quantifies the cross-sectional area and heat transfer pathway to explain that the copper particle size affects SCP's ability to transport heat. It also justifies why a range of 45–70 μm results in the maximum effective thermal conductivity for its high solid-phase cross-sectional area and shortest length of heat transfer pathway. In this instance, the analysis provided

more details but did not confirm the accuracy of the single porosity data observations for the various particle size ranges.

- In conclusion, the new correlation, using only the effective thermal conductivity measurements, reveals microstructure characteristics of SCP's solid and fluid phases in terms of cross-sectional areas, lengths of heat transfer pathways, and Langmuir shape factors related to the parallel and series heat transfer, thus providing insight and a step forward in understanding conduction heat transfer in porous media.

Acknowledgments

We gratefully acknowledge the support of Kuwait University.

References

[1] M. Kaviany, *Principles of heat transfer in porous media*. (2nd ed.). New York: Springer, (2001).
[2] Pietrak K., Wiśniewski T.S. A review of models for effective thermal conductivity of composite materials. Journal of Power Technologies 95(1), 14–24 (2015).
[3] P. Ranut, "On the effective thermal conductivity of aluminum metal foams: Review and improvement of the available empirical and analytical models," Applied Thermal Engineering 101 496–524 (2016). https://doi.org/10.1016/j.applthermaleng.2015.09.094
[4] L. Gong, Y. Wang, X. Cheng, R. Zhang, and H. Zhang, "A novel effective medium theory for modeling the thermal conductivity of porous materials," International Journal of Heat and Mass Transfer 68 295–298 (2014). https://doi.org/10.1016/j.ijheatmasstransfer.2013.09.043
[5] J. K. Carson, "Review of effective thermal conductivity models for foods," International Journal of Refrigeration, Volume 29, Issue 6, Pages 958-967 (2006).
[6] Nan C.W., Birringer R., Clarke D.R., Gleiter H. Effective thermal conductivity of particulate composites with interfacial thermal resistance. J. Appl. Phys. 81 (10), 15 May 1997. https://doi.org/10.1063/1.365209
[7] Benveniste Y., Miloh T. The effective conductivity of composites with imperfect thermal contact at constituent interfaces. Int. J. Eng. Sci. 24 (9) 1537 (1986).
https://doi.org/10.1016/0020-7225(86)90162-X
[8] Benveniste Y. Effective thermal conductivity of composites with a thermal contact resistance between the constituents: Nondilute case. J. Appl. Phys. 61 (8) 2840 (1987). https://doi.org/10.1063/1.337877.
[9] Randrianalisoa J., Baillis D., Martin C.L., Dendievel R. Microstructure effects on thermal conductivity of open-cell foams generated from the Laguerre-Voronoï tessellation method. International Journal of Thermal SP. Sciences 98, 277-286 (2015). https://doi.org/10.1016/j.ijthermalsci.2015.07.016
[10] Sumirat I., Ando Y., Shimamura S. Theoretical consideration of the effect of porosity on thermal conductivity of porous materials. J Porous Mater 13, 439–443 (2006). https://doi.org/10.1007/s10934-006-8043-0
[11] Askari R., Taheri R., Taheri S., and Hejazi H. Thermal conductivity of granular porous media: A pore-scale modeling approach. AIP ADVANCES5, 097106 (2015). https://doi.org/10.1063/1.4930258
[12] Skibinski J., Cwieka K., Ibrahim S.H., and Wejrzanowski T. Influence of pore size variation on thermal conductivity of open-porous foams. Materials, 12, 2017 (2019). https://doi.org/10.3390/ma12122017
[13] Lu X.., Zhao Y., Wang G., and Zhu X. Effects of structure characteristics and fluid on the effective thermal conductivity of sintered copper foam. Results in Physics (2020), Volume 19, 103655. https://doi.org/10.1016/j.rinp.2020.103655
[14] Ibrahim O.M., Al-Saiafi A.H., and S. Alotaibi S. Thermal conductivity of porous sintered metal powder and the Langmuir shape factor. Heat Mass Transfer (2021). https://doi.org/10.1007/s00231021-03032-x
[15] Zhao Y.Y., Fung T, Zhang L.P., Zhang F.L. Lost carbonate sintering process for manufacturing metal foams," Scripta Materialia 52 (2005) 295-298. https://doi.org.10.1016/j.scriptamat.2004.10.012
[16] Thewsey D.J, Zhao Y.T. Thermal conductivity of porous copper manufactured by the lost carbonate sintering process. Phys. Stat. Sol. (a) 205, No. 5, 1126 – 1131 (2008). https://doi.org/10.1002/pssa.200723121
[17] Corsan J.M. A compact thermal conductivity apparatus for good conductors. J. Phys. E: Sci. Instrum. 17 800 (1984). https://doi.org/10.1088/0022-3735/17/9/018